PAPER

Bimodal ion energy distribution functions in a hydrogen magnetized plasma

View the article online for updates and enhancements.

IOP ebooks™

Bringing you innovative digital publishing with leading voices to create your essential collection of books in STEM research.

Start exploring the collection - download the first chapter of every title for free.

Bimodal ion energy distribution functions in a hydrogen magnetized plasma

Osvaldo Daniel Cortázar[1] and **Ana Megía-Macías**[2]

[1] University of Castilla-La Mancha, Superior School of Industrial Engineering (ETSII), Department of Applied Mechanics, Institute for Energy Research (INEI), Av. Camilo José Cela s/n, 13071 Ciudad Real, Spain
[2] University of Deusto, Faculty of Engineering, Av. de las Universidades 24, 48007 Bilbao, Spain

E-mail: daniel.cortazar@uclm.es

Abstract
Direct measurements of temporal evolution of the ion energy distribution functions (IEDFs) in a pulsed magnetized hydrogen plasma with a complex spatial structure are presented. The results show a remarkable split of the curves into two peaks of energy that draw away as the spatial structure expands until they reach a complete separation. The behavior is explained in terms of $\boldsymbol{E} \times \boldsymbol{B}$ drift velocity plasma dynamics and its influence on the IEDFs, with consequences for ion temperature measurements. The development of a criterion to calculate the ion temperatures allows us to obtain the temporal evolution of this parameter for the three ion species, H^+, H_2^+ and H_3^+.

1. Introduction

The ion energy distribution functions (IEDFs) of the species involved in a hydrogen plasma are of interest for understanding the ion dynamics within the discharge, comparing the rates of certain plasma chemical reactions, especially in discharges of molecular species, and predicting the thermal properties of potentially extracted ion beams. While some important theoretical work has been done [1–3], the experimental results are concentrated on measurements of the electron energy distribution functions (EEDFs) due to their importance for plasma modeling [4–8]. However, data on IEDFs will provide some significant information for understanding the complex phenomena involved in the energy transfer dynamics between electrons, ions and neutrals in connection with the magnetic field for electron cyclotron resonance (ECR) plasma sources.

Measurements of time-resolved IEDFs have been reported for argon microwave/RF plasmas applied to functional coatings such as optical protective barriers and hard films in order to determine the total energy delivered by the impact of ions onto a surface [9]. Moreover, the first direct measurements of IEDFs for a hydrogen plasma have recently been published by the authors for a spatial mode configuration called 'column' where the plasma is concentrated in a symmetric cylindrical column centered in the axis of the plasma chamber [10]. However, the study of the IEDFs for cases where the plasma is anisotropically distributed is of interest because of its implications for plasma sources where it may be present, such as magnetron sputtering systems and thrusters [11, 12]. Herein we study the importance of collective phenomena in the estimation of ion temperatures of an asymmetrical distributed plasma. The study covers the first direct measurements of the temporal evolution of IEDFs for a hydrogen magnetized plasma during the entire plasma pulse, correlated with the temporal–spatial evolution of a complex plasma distribution mode called 'hourglass' [10]. The IEDFs show a remarkable split during the temporal evolution in accordance with the spreading of the spatial plasma distribution. The results suggest a collective axial velocity distribution where the influence of $\boldsymbol{E} \times \boldsymbol{B}$ drift velocity plays a key role in the IEDF dynamics, which in turn influences the calculation of ion temperature evolution for H^+, H_2^+ and H_3^+.

2. Experimental arrangement

The study was carried out in a 2.45 GHz hydrogen plasma reactor called TIPS (Test-bench for Ion source Plasma
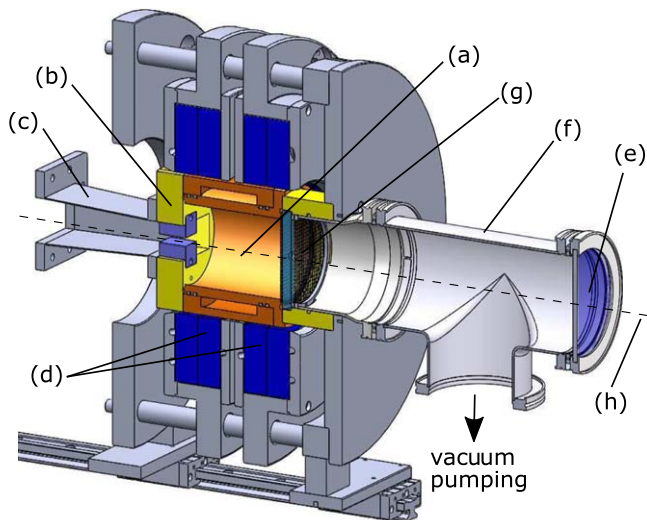
Figure 1. A cross-sectional view of the plasma reactor with the ultra-fast pictures setup: (a) plasma chamber, (b) microwave coupler, (c) microwave waveguide adapter, (d) coil pancakes, (e) quartz window placed in front of the camera, (f) vacuum tee, (g) optical window with shielding grids, (h) the optical sight axis.

Studies) [13]. The reactor operates in pulsed mode at 100 Hz with a duty cycle of 10% (1 ms pulse width). The plasma is embedded in a solenoid magnetic field produced by four axial coils that create an axial field of approximately 90 mT at the center of the plasma chamber.

Two different measurement setups have been used. The first allows one to obtain ultra-fast picture sequences to study the temporal evolution of the plasma spatial distribution modes by using a transparent microwave shielded window that works as a full metal wall while allowing the entire

plasma chamber volume to be observed [14, 15]. An ultra high-speed light-intensified frame CCD camera system is used to take up to four image sequences with independently adjusted exposure times and delays between each shot. Figure 1 shows a cross-sectional view of the setup.

The typical exposure time was 1 μs, while the delay between pictures was adjusted depending on the plasma dynamics. The gains in multi-channel plates (MCPs) and CCDs were adjusted depending on the incoming light intensity. The images were transformed through calibration into a representation where red corresponds to the highest intensity and blue to the lowest. Optical filters centered on the wavelengths of Balmer-alpha and Fulcher band emissions were been used with the ultra-fast camera system to obtain images that can be correlated with the populations of H^+ and the molecular H_2^+ and H_3^+ ions. Although the correlation between Balmer-alpha and the concentration of H^+ is not entirely correct in general terms, we assume it to be a reasonable approximation for this case on the basis of our own previous experience with simultaneous temporal measurements of ion populations and Balmer line intensity under the same experimental conditions [15].

The second setup was used to measure the temporal evolution of the IEDFs using a plasma ion mass spectrometer that uses a 45° energy sector analyzer in tandem with a quadrupole mass analyzer [16]. This configuration is able to select a particular ion (mass and charge) to measure the corresponding energy distribution. The spectrometer is capable of running energy scans from 0 to 100 eV at increments of 0.05 eV/0.25 eV full width at half maximum. The IEDFs are obtained every 5 μs with 1 μs time resolution during the entire pulse duration, and to ensure an adequate signal to noise ratio each temporal data point of the IEDF is taken over
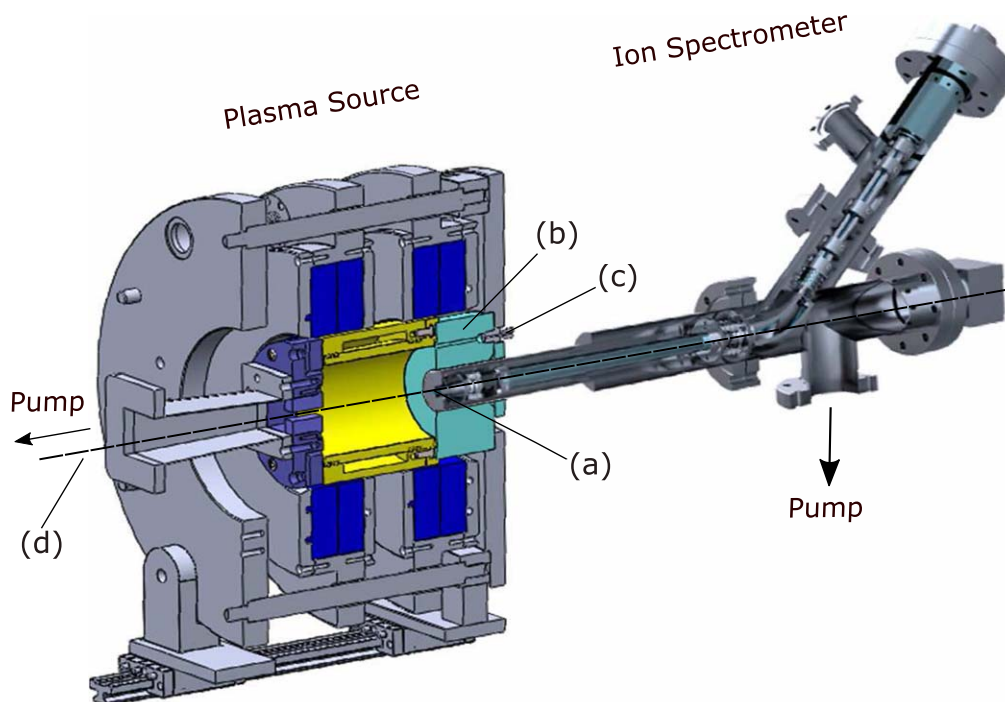
Figure 2. A cross-sectional view of the plasma reactor with the ion mass spectrometer setup: (a) 50 μm diameter extraction pinhole of the probe spectrometer, (b) adapter flange, (c) fiber optics port, (d) the optical sight axis z.

10 consecutive pulses and averaged. Figure 2 shows a cross-sectional view of the setup where the insertion of the spectrometer in the plasma source is shown. The extraction 50 μm pinhole (a) is set flush to the inner surface of the plasma chamber wall by using an adapter flange with a fiber optics port that allows a light signal to obtained from the plasma that is used for synchronization. Special attention was paid to the timing jitter and the reproducibility of the results to make the results from both setups comparable.

The acceptance angle of the spectrometer defines the region of the plasma from which the particles are coming. Equation (1) [17] explains how the distribution of velocities that the spectrometer shows as coming from the z axis actually has angular and radial components. In our case, the acceptance angle θ defines a cone of $16°$ according to the manufacturer's specifications the range of energy [18]

$$F_i(v_z) = 2\pi \int_0^{v_z \tan \theta} f_i(v_z, v_r) v_r \, \mathrm{d}v_r. \tag{1}$$

It is important to highlight this issue for this particular case because the asymmetric spatial distribution of the plasma plays a key role in the observation of the phenomenon reported herein. The capability of the spectrometer to capture particles out of the z axis allows us to understand how the energy split can be produced, as will be explained later.

As can be clearly seen by comparing figures 1 and 2, the main difference between both setups is the pumping. For the ultra-fast picture diagnostics the pumping is done through a hole of diameter 6 mm and length 10 mm in the center of the transparent shielded window. In contrast, for the ion mass spectrometer diagnostics the plasma chamber is pumped from the microwave injection side using a vacuum port in the rear microwave quartz window holder. The ion mass spectrometer has its own vacuum pumping system that can reach 10^{-7} mbar while the operational pressure in the plasma chamber is in the range of 10^{-3} mbar of flowing hydrogen.

In order to check the influence of this change in the pumping flow, several experiments with the ultra-fast picture setup were conducted by pumping the plasma chamber from the rear microwave injection side and even from both rear and front simultaneously. No appreciable differences were detected for the plasma distribution and behavior and a remarkable reproducibility was observed, as reported in [10]. This allows us to assume that the plasma characteristics remain the same for both experimental setups.

3. Results

Figure 3 shows a surface representation of a full set of normalized data obtained for the ion H$^+$ where the split can be observed. The number of particles is represented on the vertical axis by the color code, where blue is zero and yellow corresponds to the unit. The lower image is a projection of the surface on the energy–time plane.

The measurements were conducted under the experimental conditions of the plasma hourglass spatial distribution mode, although the magnetic configuration is close to the
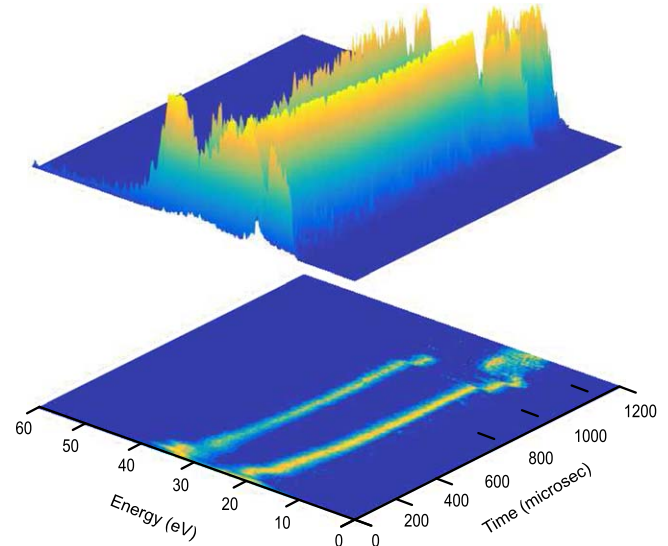
Figure 3. Normalized experimental data corresponding to the temporal evolution of the IEDF for the H$^+$ ion. The lower image is a projection of the surface on the energy–time plane.

'slug' mode, which showing some similarity to the former [10]. This mode evolves from a column shape in the center of the chamber at the discharge breakdown stage to a structure with two lobes located on the axis where the resonant microwave electric field strength is maximum during the steady-state stage [13]. Figures 4 and 5 show image sequences for Balmer-alpha emission correlated with the H$^+$ IEDFs during the aforementioned stages. In figure 4, the measurements were obtained with a temporal resolution of 1 μs for both pictures and IEDFs, with a separation of 10 μs between them. The breakdown evolves showing the formation of a bimodal IEDF after the initial 10–20 μs, in coincidence with the formation of the two characteristic lobes of the hourglass spatial distribution mode. In figure 5, the spacing between the measurements has been modified in accordance with the dynamics of the plasma. The first image was taken at 40 μs from the beginning of the microwave pulse and it is a continuation of the previous sequence. The remaining pictures in figure 5 show the evolution of the plasma distribution towards the steady state. The correlation with the IEDF evolution shows a remarkable separation of the peaks that becomes larger as the two lobes of the plasma distribution increase their area. It also noteworthy that the IEDFs obtained for H$_2^+$ and H$_3^+$ present the same behavior but we not show these data in this paper for reasons of space.

4. Analysis and discussion

These results strongly contrast with those of a previous study recently published by the authors about the IEDF temporal evolution for the column mode, where no split in the IEDFs was observed [10, 16]. For that case, the calculations of the ion temperatures were made by transforming the IEDFs into ion velocity distribution functions (IVDFs). The thermal part of the velocity distributions had to be centered at zero and the
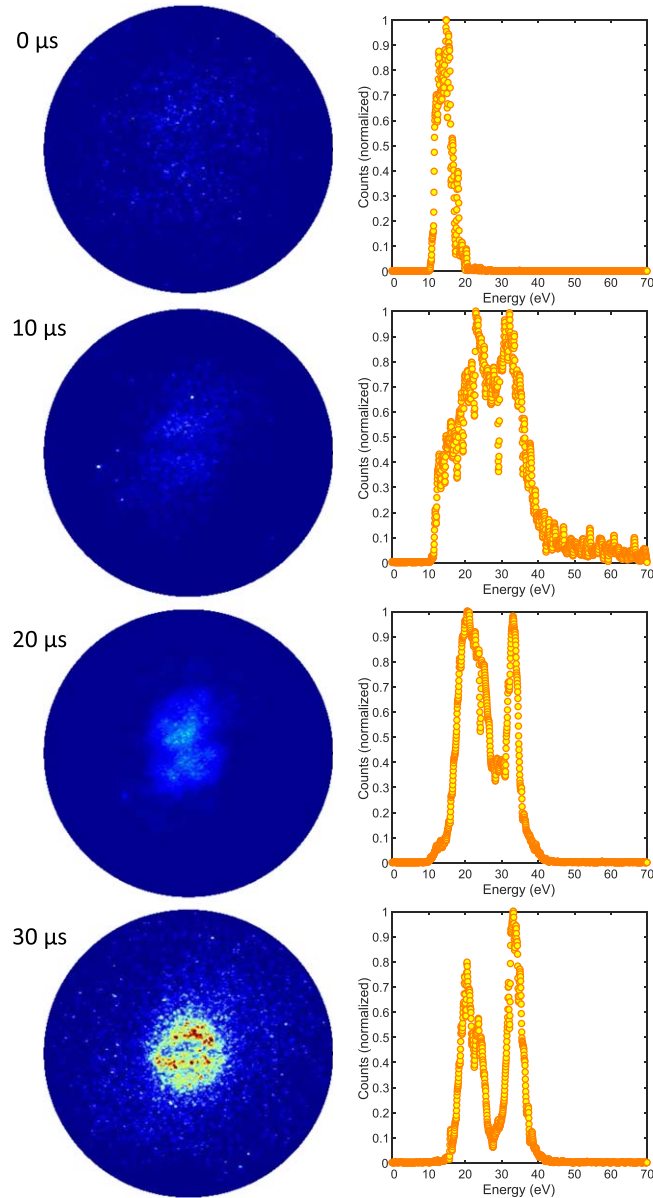
Figure 4. Image sequence of Balmer-alpha emission with corresponding IEDFs obtained during the 'breakdown' stage for H^+, with a temporal resolution of 1 μs and a separation of 10 μs.

Figure 5. Images of the Balmer-alpha emission sequence and with IEDFs corresponding to the steady-state stage for H^+.

shift in the entire curve was assumed to be due to the axial acceleration produced by the plasma potential. Such assumptions were made considering that our magnetic profile does not have the structure of a magnetic mirror (which would filter the ion escape velocities) and that the shifted distributions are (nearly) Gaussian in shape. The energy shift due to the plasma potential causes the particles entering the analyzer to have a longitudinal shift velocity v_{shift} towards the detector. The velocity distribution of the recorded ions could then be described in terms of shifted Maxwell–Boltzmann distribution. The IVDFs for an specific ion i could thus be fitted with a shifted Maxwell–Boltzmann distribution expressed in the

definition:

$$F_i(v_z) = \left(\frac{m_i}{2\pi kT_i}\right)^{\frac{3}{2}} \exp\left[\frac{-m_i(v - v_{shift})^2}{2kT_i}\right], \qquad (2)$$

where we consider the (longitudinal) shift velocity v_{shift} related to the average plasma potential V_p using the kinetic energy equation $v_{shift} = \sqrt{2qV_p/m_i}$ where q is the ion charge, i.e. the elementary charge for singly charged ions, and m_i is the ion mass.

However, in the present case of the hourglass mode, the split in the energy distribution to reach two completely separated curves during the steady-state stage in line with the spreading of the plasma space distribution, suggests the existence of a complex collective plasma velocity field which is able to provide the particles with different velocities in the axial direction (towards or away from the spectrometer). One possible explanation involves the formation of some plasma
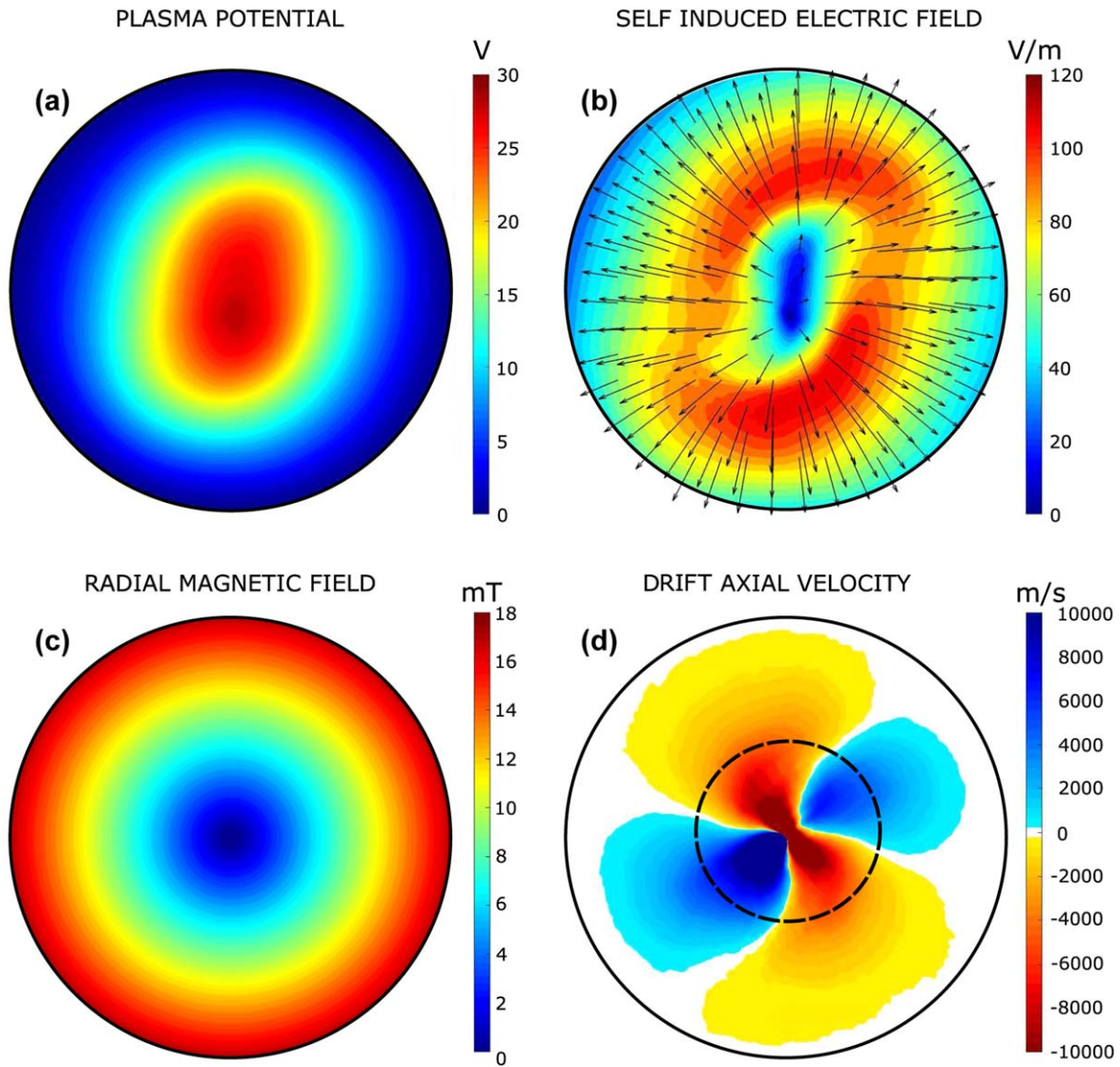
Figure 6. Calculations: (a) the plasma potential from the solution to Poisson's equation, (b) the electric field distribution, (c) the radial magnetic field on the ion mass spectrometer probe and (d) the drift velocity map obtained by $E \times B$ operation between (b) and (c), respectively. The superimposed black dashed circle represents the base of the spectrometer acceptance cone at the bottom of the plasma chamber in the experiment.

regions with opposite axial velocities. If this hypothesis is correct, these velocities could lead to a split in the IVDFs. On one hand the particles with collective axial velocity towards the detector would be measured with a velocity resulting from the sum of thermal velocity, the velocity produced by the plasma potential and the collective velocity. On the other hand, the particles with backwards axial collective velocity would be measured with a total velocity resulting from the sum of the thermal velocity and the velocity produced by the plasma potential minus the collective velocity. The IVDFs would then have two separate distributions (peaks) that would be directly reflected in the IEDFs, as is the case in the experimental data. Assuming that forward and backward axial collective velocities are equal because of symmetry, as we will check by later calculations, the central point between the two peaks should be the plasma potential (V_p). Following the previous hypothesis, the average plasma potential should be

at a point equidistant between the peaks in figures 4 and 5, i.e. $V_p \approx 27$ V in our case and the value of the v_{shift} that it produces could be estimated at about 7.3×10^4 m s^{-1}.

The parallel between the split in the plasma lobes and the split in the IEDFs points to the plasma distribution modes being a key factor. At the same time, the fact that this split in the IEDFs is observed in the hourglass mode but not in the column mode reinforces this point and suggests that the external magnetic field, in which the plasma is embedded, is most likely responsible for the phenomenon because it is the main difference between each experimental condition.

These clues induced us to investigate the split as a consequence of the complex dynamics involving an unbalanced charge distribution where the quasi-neutrality is staggered across a large scale that can reach 100–1000 λ_D (where λ_D is the Debye length), as reported in [19] and by the authors in a recent work [20]. In these works the $E \times B$ drift velocity
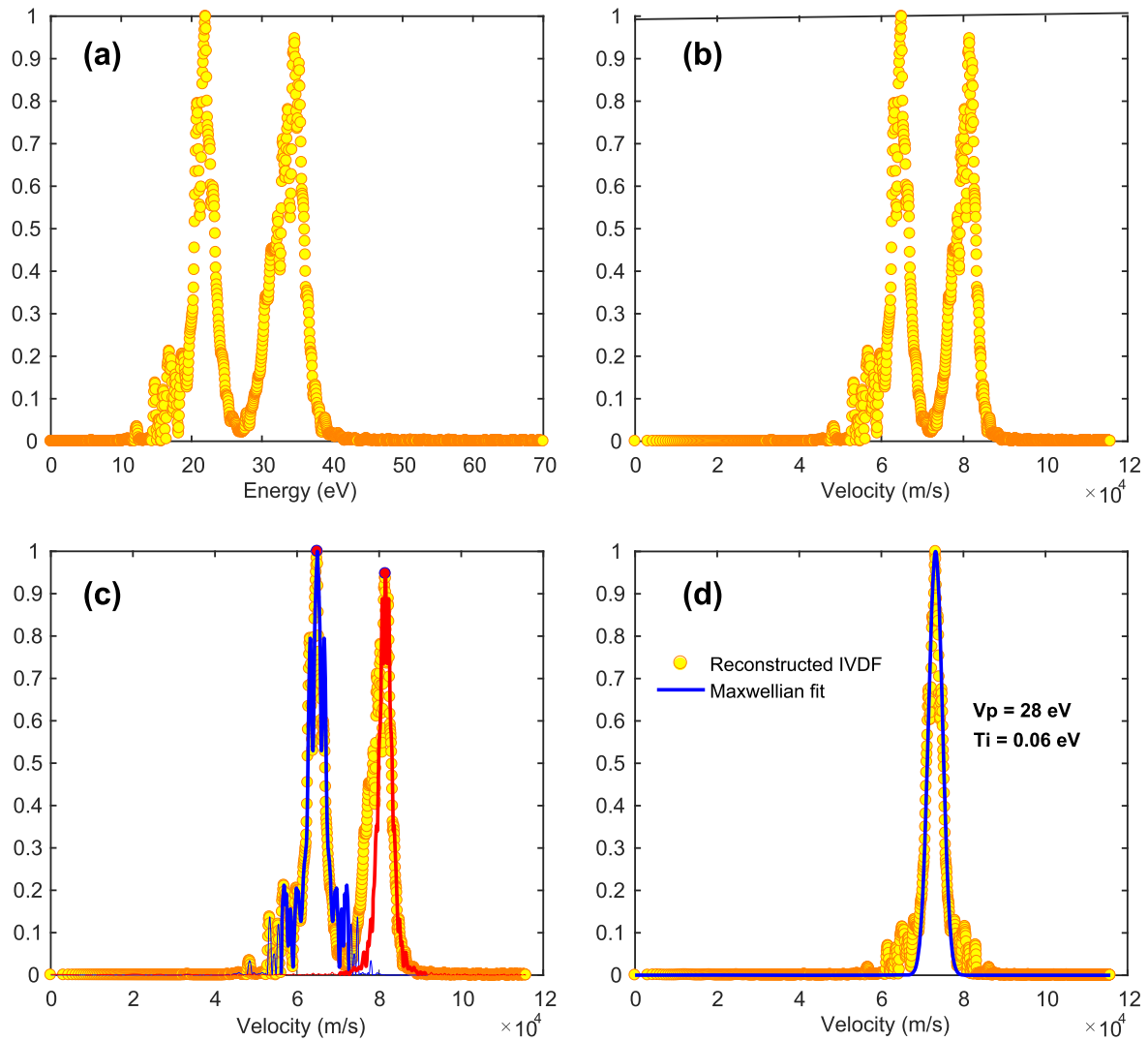
Figure 7. Data treatment of the IEDF corresponding to 70 μs.
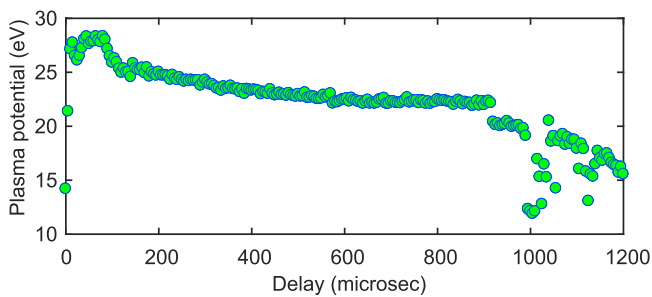
Figure 8. Temporal evolution of the plasma potential.

plays a crucial role as the main driver for collective plasma behavior and also for some instabilities related to spatial phenomena recently observed in low-temperature and low-density laboratory plasmas [21].

In our experiment, the magnetic field profile has a small radial component that is usually considered negligible because it accounts for less than 10% of the axial component. However, this radial component could play a key role in the IEDF dynamics via the $\boldsymbol{E} \times \boldsymbol{B}$ drift velocity, as proposed below.

The starting point is to suppose a radial unbalanced charge distribution $e\,(n_i - n_e) \geqslant 0$ (due to the difference in mobility between electrons and ions) which produces an electrostatic potential ϕ to reduce the electron loss rate toward the chamber wall. This potential obeys Poisson's equation $\varepsilon_0 \nabla^2 \phi = -e\,(n_i - n_e)$.

Moreover, assuming that the plasma is optically thin, the emitted light intensity can be considered proportional to the ion density point-to-point [22, 23] and the spatial distribution of light intensity can be used as a pattern for the charge distribution. A typical image can therefore be used as a positive free charge density distribution to solve Poisson's equation. Charge value calibration can be done by using the average plasma potential V_p already mentioned.

Figure 6 shows the sequence of numerical calculations that produces the map of drift axial velocities. In particular, the third picture for 70 μs in figure 5 was used as the electric charge distribution input to solve Poisson's equation with boundary conditions $\phi(R) = 0\,V$ and $\mathrm{d}\phi/\mathrm{d}r(R) = 0\,\mathrm{V}\ \mathrm{m}^{-1}$ where R is the radius of the plasma chamber. Figure 6(a) shows the calculated plasma potential. Figure 6(b) shows the
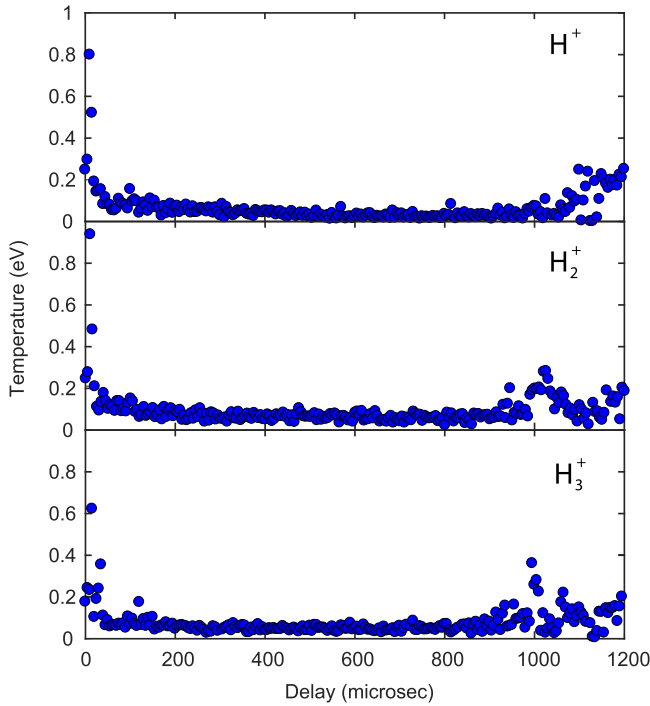
Figure 9. Evolution of the ion temperature of the three ion species H$^+$, H$_2^+$ and H$_3^+$ during the entire pulse duration.

electric field map obtained by applying the gradient to figure 6(a). Note that the electric field distribution points outwards. Figure 6(c) is the radial component of the external magnetic field applied by coils in the vicinity of extraction. Finally, figure 6(d) represents the results of $\boldsymbol{E} \times \boldsymbol{B}$ operation between 6(b) and (c), respectively, giving the map of drift axial velocity. The obtained velocity map is parallel to the plasma chamber axis and the directions are indicated by the color code, where blue corresponds to velocities towards the detector and red to velocities away from it (exiting and entering the page, respectively). The color intensity indicates the values, as shown in the scales. Note the high symmetry of the magnitudes of forward and backward velocities in accordance with our previous assumption when calculating the plasma potential as the center point between the peaks of the IEDFs. The superimposed black dashed circle in figure 6(d) represents the diameter of the base of spectrometer acceptation cone, subtended from the spectrometer pinhole as the vertex, and represents the volume from which the particles can come.

The problem of determining the plasma potential for the typical dimensions of our experiment and a plasma chamber made of metal is three-dimensional. Nevertheless, we use a two-dimensional approach to obtain a qualitative explanation that allows us to understand the problem and reach some reasonable criteria for estimating the ion temperature with our data. In spite of the two-dimensional limitation of the pictures, which present projected images of the full plasma, we consider this approach to be useful for our purposes. With this premise, the plasma potential shown in figure 6(a) was calibrated assuming the maximum value as 27 V, as previously estimated from the equidistant point in figures 4 and 5.

The maximum charge density reaches 3×10^{-7} C m^{-3}. This means that the free non-neutralized charge particle density $(n_i - n_e)$ reaches 10^{12} m^{-3}, which implies a drop in n_e by four orders of magnitude with respect to typical measured values. Considering that λ_D is typically about 0.1 mm for this kind of plasma in conditions of quasi-neutrality, the actual length scale for the present case of quasi-neutrality breakage is estimated at $100\lambda_D \approx 10$ mm, which fits well with the plasma dimensions. The values for the electric field reach a maximum of 120 V m^{-1} and axial drift velocities $\pm 1 \times 10^4$ m s^{-1}. Therefore, the peaks in the IVDF should be at $v_{shift} \pm v_{drift}$, which in our case is $(7.3 \pm 1.0) \times 10^4$ m s^{-1}. Figures 7 (a) and (b) show the IEDF of the picture used for the previous calculations and its transformation to IVDF, respectively. There is a remarkable agreement between the positions of the peaks and the previous calculations.

To calculate the ion temperature, both peaks have to be superimposed, added and centered on v_{shift}. For cases where the peak separation produces overlap, for example the third picture in figure 4, symmetrization was done using the data of the left and right parts of the curves that are not affected. Figure 7 (c) shows the symmetrization of the left peak in blue and the right peak in red. Figure 7 (d) shows the final result once both peaks have been symmetrized, superimposed and added to the central point determined by v_{shift}. By using this technique, calculations of the ion temperature and plasma potential can be done using equation (2) for the entire ensemble of data. Figure 8 shows the temporal evolution of the plasma potential where the value for the steady-state stage is established at 24–25 V. Figure 9 shows the temporal evolution of H$^+$, H$_2^+$ and H$_3^+$ species calculated throughout the pulse. The values are typically 0.1 eV during the steady-state stage, showing peaks at the beginning of the pulse between 0.6 eV and 0.9 eV. The observation of this peaking behavior agrees with previous measurements of time-resolved electron temperatures [24]. Another lower and wider peak is observed during the pulse decay and may be associated with the well known 'afterglow' phenomenon in ECR ion sources [25].

5. Conclusions

In summary, this paper presents the first direct measurements of the temporal evolution of the ion energy distribution function (IEDF) in a pulsed magnetized hydrogen plasma with a complex spatial structure. The split of the curves into two peaks of energy whose distance apart increases as the spatial structure expands is explained in terms of the influence of $\boldsymbol{E} \times \boldsymbol{B}$ drift velocity on the plasma dynamics. This enables criteria to be developed for calculating the evolution of ion temperature for the three ion species H$^+$, H$_2^+$ and H$_3^+$ for the first time where peaks are observed during the breakdown and decay.

It is important to highlight that the effect of $\boldsymbol{E} \times \boldsymbol{B}$ drift velocity is well known in ion plasma thrusters [26] and plasma sources for fusion devices [27]. However, its influence

in the IEDF and consequences for ion temperature measurements are studied here for first time. Finally, we would like to mention that laser-induced fluorescence is an important alternative diagnostic to confirm the ion drift effects reported in this work [28–30].

Acknowledgments

ORCID iDs

Osvaldo Daniel Cortázar ● https://orcid.org/0000-0002-3930-2685

References

[1] Chen C, Wei T, Collins L R and Phillips J 1999 *J. Phys. D: Appl. Phys.* **32** 688–98
[2] Kawuamura E, Vahedi V, Lieberman M and Birdsall C 1999 *Plasma Sources Sci. Technol.* **8** R45–64
[3] Godyak V and Demidov V 2011 *J. Phys. D: Appl. Phys.* **44** 233001
[4] Bretagne J, Graham W and Hopkins M 1991 *J. Phys. D: Appl. Phys.* **24** 668–71
[5] Hopkins M and Graham W 1991 *J. Appl. Phys.* **69** 3461–6
[6] Jauberteau J, Jauberteau I, Cortázar O and Megía-Macías A 2016 *Phys. Plasmas* **23** 3513
[7] Aleiferis S, Svarnas P, Béchu S, Tarvainen O and Bacal M 2018 *Plasma Sources Sci. Technol.* **27** 075015
[8] Kalita D, Kakati B, Kausik S, Saikia B and Bandyopadhyay M 2018 *Eur. Phys. J.* D **72** 74
[9] Zabeida A, Hallil A, Wertheimer M and Martinu L 2010 *J. Appl. Phys.* **88** 635–42
[10] Cortázar O, Megía-Macías A, Tarvainen O, Vizcaíno-de Julián A and Koivisto H 2014 *Plasma Sources Sci. Technol.* **23** 065028
[11] Boeuf J 2015 *Front. Phys.* **2** 74
[12] Matjaz P, Loquai S, Klemberg-Sapieha J and Martinu L 2015 *Plasma Sources Sci. Technol.* **24** 065010
[13] Megía-Macías A, Cortázar O D and Vizcaíno-de Julián A 2014 *Rev. Sci. Instrum.* **85** 033310
[14] Cortázar O, Megía-Macías A, Vizcaíno-de Julián A, Tarvainen O, Komppula J and Koivisto H 2014 *Rev. Sci. Instrum.* **85** 02A902
[15] Cortázar O, Megía-Macías A, Tarvainen O, Kalvas T and Koivisto H 2016 *Rev. Sci. Instrum.* **87** 02A704
[16] Megía-Macías A, Cortázar O, Tarvainen O and Koivisto H 2017 *Phys. Plasmas* **24** 113501
[17] Ong P and Hogan M 1985 *J. Phys. B: At. Mol. Phys.* **18** 1897–906
[18] HIDEN Analytical Ltd., http://hidenanalytical.com/
[19] Tanaka M and Yoshimura S 2008 *IEEE Trans. Plasma Sci.* **36** 1224–5
[20] Cortazar O and Megia-Macias A 2016 *IEEE Trans. Plasma Sci.* **44** 734–7
[21] Boeuf J and Chaudhury B 2013 *Phys. Rev. Lett.* **111** 155005
[22] Griem H R 1997 *Principles of Plasma Spectroscopy* (New York: Cambridge University Press) pp 248–50
[23] Bluem E, Béchu S, Boisse-Laporte C, Leprince P and Marec J 1995 *J. Phys. D: Appl. Phys.* **28** 1529–33
[24] Cortázar O, Megía-Macías A and Vizcaíno-de Julián A 2012 *Rev. Sci. Instrum.* **83** 3302
[25] Cortázar O, Megía-Macías A and Vizcaíno-de Julián A 2013 *Rev. Sci. Instrum.* **84** 093301
[26] Adam J *et al* 2008 *Plasma Phys. Control. Fusion* **50** 1–17
[27] Fubiani G, Garrigues L, Hagelaar G, Kohen N and Boeuf J 2017 *New J. Phys.* **19** 015002
[28] Amorim J and Jolly J 2000 *J. Phys. D: Appl. Phys.* **33** R51–65
[29] Kim J and Lee H 2006 *J. Korean Phys. Soc.* **49** S184–6
[30] Liebeskind J, Hanson R and Cappelli M 1993 *Appl. Optics* **32** 6117–27